Spontaneous formation of multilayer refractory carbide coatings in a molten salt media

Loic Constantin[a,b,1], Lisha Fan[a], Mathilde Pouey[b], Jérôme Roger[c], Bai Cui[d], Jean-François Silvain[a,b,1], and Yong Feng Lu[a,1]

[a]Department of Electrical and Computer Engineering, University of Nebraska–Lincoln, Lincoln, NE, 68588-0511; [b]CNRS, Bordeaux INP, Institut de Chimie de la Matière Condensée de Bordeaux (ICMCB), UPMR 5026, Université of Bordeaux, F-33608 Pessac, France; [c]Laboratoire des Composites Thermo Structuraux–LCTS 3 allée de la Boétie, Université de Bordeaux, F-33600 Pessac Cedex, France; and [d]Department of Mechanical and Materials Engineering, University of Nebraska–Lincoln, Lincoln, NE 68588-0526

Edited by Alexis T. Bell, University of California, Berkeley, CA, and approved March 29, 2021 (received for review January 12, 2021)

Refractory materials hold great promise to develop functional multilayer coating for extreme environments and temperature applications but require high temperature and complex synthesis to overcome their strong atomic bonding and form a multilayer structure. Here, a spontaneous reaction producing sophisticated multilayer refractory carbide coatings on carbon fiber (CF) is reported. This approach utilizes a relatively low-temperature (950 °C) molten-salt process for forming refractory carbides. The reaction of titanium (Ti), chromium (Cr), and CF yields a complex, high-quality multilayer carbide coating composed of 1) Cr carbide (Cr_3C_2), 2) Ti carbide, and 3) Cr_3C_2 layers. The layered sequence arises from a difference in metal dissolutions, reactions, and diffusion rates in the salt media. The multilayer-coated CFs act as a permeable oxidation barrier with no crystalline degradation of the CFs after extreme temperature (1,200 °C) and environment (oxyacetylene flame) exposure. The synthesis of high-quality multilayer refractory coating in a fast, efficient, easy, and clean manner may answer the need for industrial applications that develop cheap and reliable extreme environment protection barriers.

molten salt synthesis | oxidation barrier | multilayer coating | refractory carbide | carbon fibers

Carbon fibers (CFs) are strong, lightweight, and have the unique capability to hold their mechanical properties at elevated temperatures (up to 2,500 °C) (1, 2). These unmatched properties have drawn significant interest for extreme environmental and temperature applications (3–5). However, the weak oxidation/fire resistance of CFs (~400 °C) requires protection against harsh environments (6). Since the late 1930s, extensive research efforts have been undertaken to develop an inexpensive and reliable oxidation barrier made of refractory oxides, nitrides, and carbides (5, 7, 8). Among them, refractory carbides have gained consideration because of their spontaneous reaction with C, high melting point, and excellent oxygen permeability (9–11). Substantial evidence suggests that materials coated in multiple carbide layers possess superior resistance to oxidation and ablation than traditional single-layer carbide coatings (12–14). Combining different carbides into a multilayer forms a passive layer on the coating surface, enhancing the overall oxidation resistance (15). Nevertheless, the synthesis of a multilayer carbide coating needs elevated temperatures to overcome the strong atomic bonding of the carbide and requires complex and costly synthesis methods for forming a multilayer structure (16).

Unlike conventional solid- and liquid-state synthesis, molten salt synthesis (MSS) offers a fast, easy, and affordable method of synthesizing refractory materials (17). When heated above the melting point, the ionic nature of the molten salt destabilizes the atomic bonds, facilitating the chemical reactions and lowering the reactional temperature (18). Acting as a solvent, the molten salt enhances the transport and diffusion of dissolved species, leading to the fast synthesis of refractory materials. In addition, the aqueous solubility of the salt ensures easy removal of the solid solvent at the end of the reaction and recovery of the final product, making the MSS process clean and scalable (11). To date, a wide range of refractory carbides have been coated on carbon materials via MSS, including TiC, ZrC, SiC, and TaC (19–22). It was reported that refractory carbides synthesized by an MSS process possess high purity with tribological and mechanical properties like those obtained by conventional chemical vapor deposition (23, 24). MSS processes have therefore proven to be easy, cost-effective, and clean methods of synthesizing single-layer coatings of refractory carbides and could in a similar fashion be used to produce multilayer carbide coatings.

Here, we present a spontaneous and low-temperature reaction using a single-step molten salt process to form a multilayer refractory carbides coating on CFs. Our study focused on TiC and Cr_3C_2 due to their excellent wear, oxidation, and erosion resistance (25). Analyses of the microstructure and chemical properties of the synthesized multilayer carbides revealed three distinct layers composed of Cr_3C_2–TiC–Cr_3C_2. To better understand the reaction involves in the formation of the complex multilayer coating, rapid quenching of the molten salt and kinetic analyses of TiC and Cr_3C_2 single layers were performed. It is shown that the coatings undergo a kinetic control during the first minutes of the process that enables the formation of a complex sequence. Finally, the multilayer-coated CFs showed

Significance

Multilayer coatings of refractory materials are of significant interest for extreme environment applications. Yet, the strong covalent bonding of refractory materials and the complexity of synthesizing multilayer structures impedes their development. Our work presents a fast, easy, and low-temperature synthesis of complex multilayer carbide coatings via a spontaneous reaction in a molten salt media. The synergistic reactions that yield the multilayer coating on carbon fibers depend on metal dissolution and diffusion in the salt media. We demonstrate that the synthesized multilayer coating possesses superior harsh environment resistance compared to single-layer coatings. The proposed synthesis method provides an effective route of producing complex oxidation barriers in an easy, scalable, and affordable manner, holding great promise for developing functional coatings.

Author contributions: L.C., J-F.S., and Y.F.L designed research; L.C. and M.P. performed research; L.C., L.F., J.R., B.C., J.-F.S., and Y.F.L. analyzed data; and L.C., L.F., J.-F.S., and Y.F.L. wrote the paper.

The authors declare no competing interest.

This article is a PNAS Direct Submission.

[1]To whom correspondence may be addressed. Email: constantin.loic@gmail.com, jean-francois.silvain@icmcb.cnrs.fr, or YLU2@UNL.EDU.

This article contains supporting information online at https://www.pnas.org/lookup/suppl/doi:10.1073/pnas.2100663118/-/DCSupplemental.

Published April 26, 2021.

extreme temperature and environment resistance when subjected to an oxyacetylene flame as compared to the single-coated CFs. MSS enables, thus, the formation of a complex and high-quality multilayer refractory coating in a rapid, efficient, and clean manner, holding great promise to produce low-cost and reliable environmental barriers.

Results and Discussion

KCl has the ability to dissolve both Cr and Ti metallic powders (26, 27). Therefore, KCl was used as the reaction media in this work at 950 °C for 5 h. Note a temperature of 950 °C is considered relatively low due to elevated temperatures (>1,000 °C) required to synthesize Ti and Cr carbides (28–30). After the MSS process, the salt was washed away in boiling water (*SI Appendix*, Fig. S1). Then, the surface microstructure of the CFs was observed by scanning electron microscopy (SEM) with a back-scattered electron (BSE) mode to enhance the contrast between the CFs and the coated layers.

Fig. 1*A* and *SI Appendix*, Fig. S2 show the fibers coated using metal (M) = Ti, M = Cr, and M = Ti + Cr and reveals homogenous layers on all CFs throughout the anisotropic structure of about 600 nm. The coating obtained with M = Ti and M = Cr was a monocontrasted layer, implying a single-phase formation, as shown in Fig. 1*B*. The deposition of single-carbide coating is confirmed in the X-ray diffractograms (Fig. 1*C*). When M = Ti, the diffractogram shows peaks at 2θ = 35.9, 41.7, 60.4, 72.3, and 76.1°, corresponding to the (111), (200), (220), (311), and (222) planes of cubic phase, suggesting the formation of TiC (powder diffraction file [PDF] card 31-1400). Then, when M = Cr, the pattern shows peaks at 2θ = 32.6, 35.2, 36.0, 39.0, 40.2, 42.6, 45.5, 46.6, 47.4, 48.6, 50.1, 51.2, 66.0, and 76.3°, attributing to the (011), (140), (220), (121), (230), (150), (240), (211), (060), (221), (310), (051), (002), and (181) planes of orthorhombic phase, adumbrate the formation of Cr_3C_2 (PDF card 14-406).

In opposition, when M = Ti + Cr, two contrasted layers were observed, suggesting the formation of two phases, as illustrated in Fig. 1*B*. The diffractogram displays peaks attributed to both Cr_3C_2 and TiC, indicating the formation of a multilayer carbide coating. We then analyzed the multilayer coating's elemental and chemical composition by Auger electron spectroscopy (AES) depth profiling to get more insight into the coating sequence, as shown in Fig. 1*D*. The atomic concentrations of Cr, Ti, and C match the formation of three distinct layers; 1) Cr_3C_2, 2) TiC, and 3) Cr_3C_2 and corroborates the BSE and X-ray diffraction observations. Additionally, the AES depth profile reveals that the TiC layer has a stichometry comprise between $TiC_{0.8}$ and $TiC_{0.85}$. At the same time, Cr_3Cr_2 (~66 AT% C) is the only Cr carbide presents in the multilayer coating, as shown in Fig. 1*D*. Also, no trace of Cr was detected in the TiC layer and vice versa, suggesting that no diffusion of Cr in the TiC occurred at 950 °C, regardless of the nonnegligible solubility of Cr_3C_2 in TiC at high temperatures (>1,300 °C) (31, 32). These results indicate that complex multilayer carbide coatings can be formed using a single-step molten salt process at a low temperature (950 °C).

Next, to understand how the layer sequence is formed in molten KCl, we froze the liquid salt containing Ti + Cr – CFs at a different stage of the MSS process by air quenching. Fig. 2*A* shows a SEM micrograph of the salt quenched in the early stage

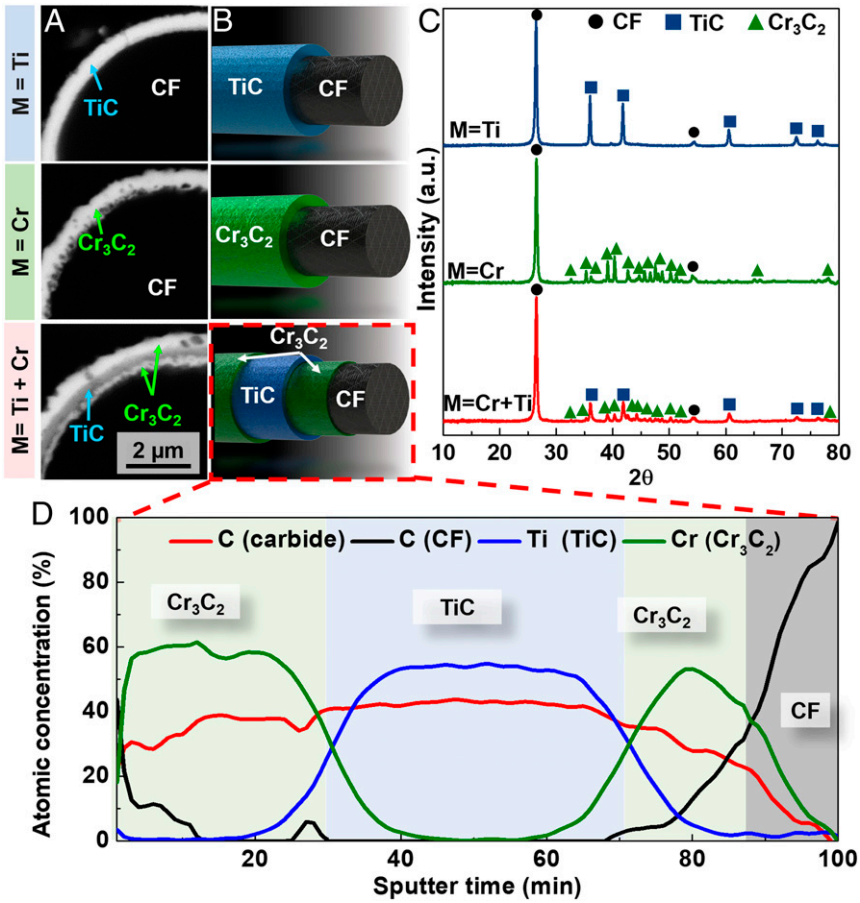

Fig. 1. SEM micrographs of Ti, Cr, and Ti + Cr coatings on CFs after the MSS: (*A*) cross-sectional views; (*B*) schematic illustrations of the coatings with M = Ti, Cr, and Cr+Ti; (*C*) XRD diffraction patterns of TiC, Cr_3C_2, and TiC + Cr_3C_2 coatings; and (*D*) AES depth profiles of the CFs coated in a Ti + Cr salt solution.

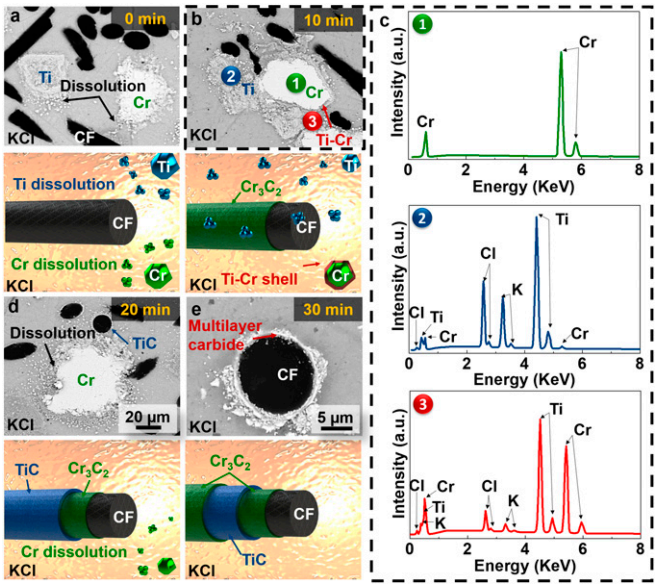

Fig. 2. Steps to form the multilayer coating: (*A* and *B*) SEM micrographs after salt quenching at different times of 0 and 10 min with illustrations, (*C*) EDX analysis of the salt quenched at 10 min, and (*D* and *E*) SEM micrographs after salt quenching at different times of 20 and 30 min with illustrations.

of the coating process. As can be observed, submicrometer Ti and Cr particles formed within a few seconds, suggesting their dissolution in the molten salt. An X-ray diffraction (XRD) analysis of the coated fibers (*SI Appendix*, Fig. S3) showed peaks corresponding to both Cr_3C_2 and TiC phases, indicating that the salt bath significantly reduced the reaction time, similar to an analysis reported by Tohru Arai et al. (33).

After 10 min (Fig. 2*A*), the number of Ti particles decreased as they transformed into TiC. However, it can also be observed that a shell surrounding the Cr particles was formed. To define the chemical compositions of this shell encapsulating the Cr particles, we analyzed three positions by energy-dispersive X-ray spectroscopy (EDX): 1) the Cr particle, 2) the Ti particle, and 3) the envelope as shown in Fig. 2*C*. The EDX spectrum of Point 1 shows the peaks corresponding to Cr. The analysis of Point 2 identifies the presence of Ti and a small amount of Cr. Finally, Point 3 indicates the presence of both Ti and Cr with a composition of about 45 AT% Ti and 55 AT% Cr. These observations suggest that while Ti reacts with the CFs to form TiC, it simultaneously reacts with Cr to form the Ti–Cr shell around the Cr particles. The Ti–Cr system binary phase diagram shows that at a molar fraction of about 0.55 Cr and 0.45 Ti, two phases can be obtained; temperatures below 1,272 °C yield both Cr_2Ti and Ti phases, and temperatures above 1,272 °C lead to Ti–Cr solid solutions (34). The XRD diffractogram obtained after 10 min of coating (*SI Appendix*, Fig. S3) shows peaks corresponding to Ti and Cr metals with traces of oxides due to the air quenching but no trace of Cr_2Ti. Reaction via a molten salt is well known to lower the synthesis temperature, and thus a coating temperature of 950 °C could suffice to form a Ti–Cr solid solution. Fig. 2*D* shows the salt mixture quenched after 20 min. The Ti particles and the shells around the Cr particles were no longer observable, suggesting their complete reaction. After 30 min, Cr powders dissolved in the salt, forming the outer Cr_3C_2 layer (Fig. 2*E*).

To clarify the formation of the first Cr_3C_2 layer during the early stage of the coating, we studied the kinetic growth of single-carbide coatings (i.e., M = Ti and M = Cr) at different temperatures and times. The kinetic analysis details can be found in *SI Appendix*, section S2 and S3 and Figs. S4–S6). Fig. 3*A* shows the measured D_{eff} for TiC and Cr_3C_2 as a function of the coating temperature. At 950 °C, D_{eff} was measured to be 1.3×10^{-12} and 4.4×10^{-12} cm^2/s for TiC and Cr_3C_2, respectively. Both values agreed well with C diffusion in TiC and Cr_2C_3 reported by both Himbeault et al. and Koyama et al., respectively (35, 36). Therefore, C diffuses three times faster in Cr_3C_2 at 950 °C than in TiC, which can explain why Cr_3C_2 formed first, as illustrated in Fig. 3*B*.

The counter diffusion of C in TiC and in Cr_3C_2 was then qualitatively observed based on the Kirkendall-induced porosity effect. This effect is a well-known phenomenon in which pores form near the reactional interface to counteract the unequal flow created by two materials with different diffusion rates (37). As illustrated in Fig. 3*C*, once pores formed, the surface diffusion became the driving force and led to channels (38). To observe the Kirkendall-induced porosity effect, we grew TiC and Cr_3C_2 layers for 7 h at 950 °C via a MSS process containing a large excess of metal. Fig. 3*D* shows that in the case of a TiC layer, pores formed at the TiC/CF interface with a remaining CF diameter of 7 μm (~10 μm initially). In contrast, in the Cr_3C_2 situation, channels formed near the Cr_3C_2/CF interface, and the CF diameter was reduced to 5 μm (Fig. 3*E*). These observations indicate that C has faster reaction and diffusion in Cr_3C_2 when produced by the MSS process than in TiC, thus supporting our kinetic analyses.

After synthesizing single and multilayer carbide coatings via an MSS process, we tested their extreme environmental resistance using an oxyacetylene flame. The coated CFs (M = Ti, Cr, and Ti+Cr) having a coating thickness of about 600 nm were glued onto a WC substrate and subjected to an oxyacetylene flame at 10 mm from the inner cone (T_{CFs} ~1,200 °C) for 60 s, as illustrated in Fig. 4*A*.

As shown in Fig. 4*B*, after the MSS process, the TiC coating surface (i.e., M = Ti) was smooth and dense. However, once subjected to the flame, particle-like features appeared on the TiC layer's surface, indicating TiC oxidation in TiO_2 (*SI Appendix*, Figs. S7*A* and S8). A cross-section of the coated fibers showed that the CFs were not completely vaporized but delaminated at the TiC/CF interface. In a similar manner, the initially smooth surface of the Cr_3C_2 layer (i.e., M = Cr) became porous after the oxidation test, leading to complete decomposition of the CFs (Fig. 4*C* and *SI Appendix*, Figs. S7*B* and S9). On the contrary, the multilayer carbide coating, M = Ti + Cr, showed only a partial erosion of the outer Cr_3C_2 after the oxyacetylene flame oxidation (Fig. 4*D* and *SI Appendix*, Fig. S7*C*). The CFs remained unchanged with an intimate CF–coating interface, as shown in *SI Appendix*, Fig. S10. The outer Cr_3C_2 layer partially oxidized, creating a passive layer, thus allowing the TiC layer and the inner Cr_3C_2 layer to protect the CFs from the extreme environment. Next, we evaluated the graphite crystallinity of the CFs before and after being subjected to the flame to further characterize the protective efficiency of the multilayer coating. The graphitization was measured based on the D- (~1,350 cm^{-1}, related to defects and disorder in the carbon structure) and G-band (~1,580 cm^{-1}, results from the ordered graphitic structure) ratio (I_D/I_G) (*SI Appendix*, Fig. S11) (39). It was found that I_D/I_G was ~0.90 for the original and after fire exposure of the CFs, implying conservation of the graphite crystallinity of the CFs.

Conclusion. In summary, an MSS process allows the synthesis of a complex multilayer coating of refractory carbides on carbon materials via a spontaneous and low-temperature reaction. The coating sequence results from differences in the dissolution, transport, diffusion, and reaction of metals in the molten salt and CFs. The resulting complex multilayer coating shows an extreme temperature and environmental resistance, which is superior to a single-carbide

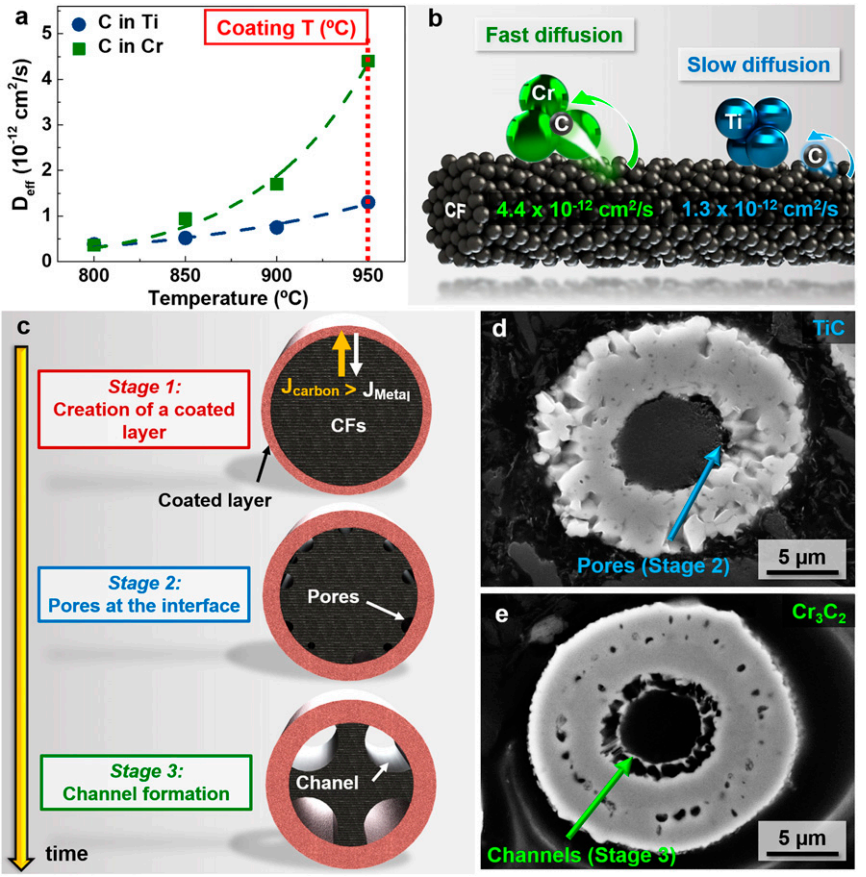

Fig. 3. Calculations and observations of C diffusion in Ti and Cr: (*A*) C diffusion coefficients in both Ti and Cr as functions of the coating temperature, (*B*) a schematic illustration of the C diffusion, and (*C*) a schematic illustration of the Kirkendall effect and coatings at 950 °C for 7 h with $n_M = n_C$ for M = (*D*) Ti and (*E*) Cr, respectively.

coating and confirms the advantage of a multilayer oxidation barrier. We hope the efficiency, simplicity, and affordability of the MSS process will open new avenues to producing functional oxidation barriers coating for a wide spray used in extreme environmental applications.

Materials and Methods

Preparation of Single and Complex Multilayer Carbide Coatings. Short polyacrylonitrile CFs with an average length of 200 µm and a diameter of 10 µm (Mitsubishi Chemical DIALEAD K223HM) were used to coat carbide layers using a molten salt process. *SI Appendix*, Fig. S1 is a schematic illustration of the different steps involved in a molten salt coating process. First, the salt (KCl), GPR Rectapur 99%) and the metal (Ti, 99.5%, mean diameter 40 µm, Cr, 99.5%, mean diameter 45 µm, or Cr + Ti) were homogeneously mixed using an agate mortar. A molar ratio of C:KCl = 1:0.6 was used in all experiments. The molar ratios for Ti, Cr, and Ti + Cr carbide coatings were C:Ti = 1:0.12, C:Cr = 1:0.12, and C:Cr:Ti = 1:0.06:0.06, respectively. The CFs were then introduced into the salt/metal mixture and manually shaken. Subsequently, the mixture was deposited on an alumina crucible, as shown in Step 1. The crucible was placed in a tubular furnace under an argon flux at a temperature ranging from 800 to 950 °C for different time periods, ranging from 0.5 to 5 h, as illustrated in Step 2. The heating and cooling rates were about 7 and 15 °C/min, respectively. When the oven cooled down, the salt was dissolved in boiling water. The coated CFs were recovered by filtration, as illustrated in Steps 3 and 4. Finally, the coated CFs were dried in an oven at 60 °C for 1 h.

Formation of Multilayer Coatings. The process to form multilayer carbide coatings was followed by air quenching the crucible at 950 °C at various times ranging from 0 to 30 min. A piece of KCl/Ti-Cr/CFs was embedded in a polyphenolic resin, which was polished and analyzed using SEM. The growth kinetic of TiC and Cr_3C_2 on CFs was studied using the ratios of C:Ti = 1:0.24 and Cr:C = 1:0.24. The coating temperatures and times varied from 800 to 950 °C and 1 to 5 h, respectively. The thickness variation of the coated layers was measured based on the cross-sectional views of the CFs. The Kirkendall

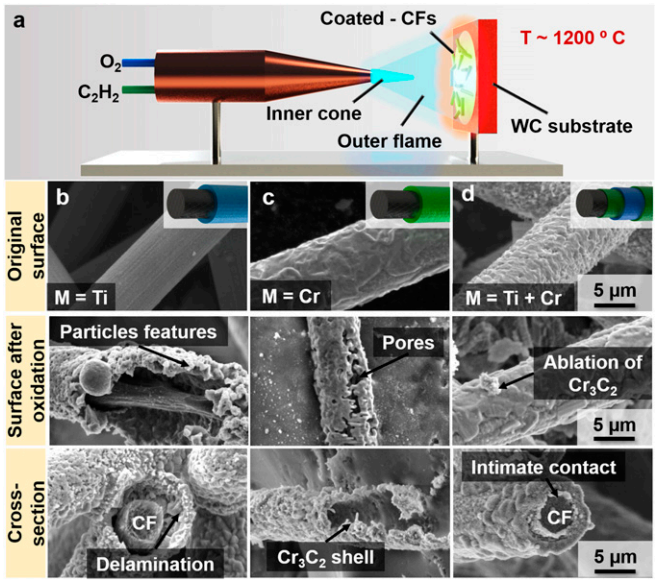

Fig. 4. Extreme environment performance of single and multilayer coatings on CFs: (*A*) a schematic illustration of the high velocity and temperature gas erosion. SEM micrographs before and after testing for (*B*) TiC, (*C*) Cr_3C_2, and (*D*) Cr_3C_2/TiC/Cr_3C_2 coatings.

effect was studied by producing a thick coating with an equimolar mixture of metal and carbon (i.e., C:Ti = 1:1 and C:Cr = 1:1) at 950 °C for 7 h.

Erosion/Oxidation under an Oxyacetylene Flame. A combustion torch with a 1.5 mm orifice was used to produce the flame. The precursor gases were a mixture of 99.6% acetylene (C_2H_2) and 99.9% oxygen (O_2) with flow rates of 1,780 and 1,800 sccm, respectively. Coated CFs were glued onto a WC substrate containing 6% of cobalt (Co) (dimensions: 12.5 × 12.5 × 1.6 mm^3). Samples were placed on a water-cooled brass stage 10 mm beneath the tip of the flame for 60 s. The temperature was evaluated by a noncontact pyrometer (OS3752, Omega Engineering, Inc.) and measured to be 1,200 °C.

Sample Characterization. Compositions of the coatings were characterized by XRD (PANalytical X'pert PRO MPD, λ = 1.5405 Å), EDX (Apollo X, EDAX Inc.), and AES (Auger VG Microlab 310 F). Surface and cross-sectional views of the CFs with different carbide coatings were analyzed by SEM using the BSE mode (VEGA II SBH, TESCAN). To obtain the cross-sectional views, the samples were encased in a polyphenolic resin and polished prior to the SEM analyses. After being subjected to the oxyacetylene flame, the oxidation state and crystallinity of the coated CFs were investigated using a micro-Raman spectrometer (inVia, Renishaw). An Ar^+ion laser with a wavelength of 514.5 nm and a power of 50 mW was used as the excitation source. The beam was focused using a 50× objective lens to ∼5 μm.

Data Availability. All study data are included in the article and/or *SI Appendix*.

ACKNOWLEDGMENTS. This research was performed in part in the Nebraska Nanoscale Facility: National Nanotechnology Coordinated Infrastructure and the Nebraska Center for Materials and Nanoscience, which are supported by the NSF under Award Electrical, Communications and Cyber Systems 1542182, and the Nebraska Research Initiative. We thank Jamie Eske for her editing to the manuscript.

1. S. Chand, Carbon fibers for composites (A review). *J. Mater. Sci.* **35**, 1303–1313 (2000).
2. T. K. Das, P. Ghosh, N. Ch. Das, Preparation, development, outcomes, and application versatility of carbon fiber-based polymer composites: A review. *Adv. Compos. Hybrid Mater.* **2**, 214–233 (2019).
3. G. Savage, "Applications of carbon-carbon composites" in *Carbon-Carbon Composites*, G. Savage, Ed. (Springer Netherlands, 1993), pp. 323–359.
4. F. Smeacetto, M. Salvo, M. Ferraris, Oxidation protective multilayer coatings for carbon–carbon composites. *Carbon* **40**, 583–587 (2002).
5. C. Friedrich, R. Gadow, M. Speicher, Protective multilayer coatings for carbon–carbon composites. *Surf. Coat. Tech.* **151–152**, 405–411 (2002).
6. C. Verdon, O. Szwedek, S. Jacques, A. Allemand, Y. Le Petitcorps, Hafnium and silicon carbide multilayer coatings for the protection of carbon composites. *Surf. Coat. Tech.* **230**, 124–129 (2013).
7. M. P. Bacos, Carbon-carbon composites: Oxidation behavior and coatings protection. *J. Phys. IV France* **03**, C7-1895-C7-1903 (1993).
8. N. P. Padture, Advanced structural ceramics in aerospace propulsion. *Nat. Mater.* **15**, 804–809 (2016).
9. O. Ledain *et al*., Reactive chemical vapour deposition of titanium carbide from H2-TiCl4 gas mixture on pyrocarbon: A comprehensive study. *Phys. Procedia* **46**, 79–87 (2013).
10. Y. Zhang, H. Li, K. Li, J. Fei, X. Zeng, C/SiC/Si-Mo-Cr multilayer coating for carbon/carbon composites for oxidation protection. *N. Carbon Mater.* **27**, 105–109 (2012).
11. A. Dash, R. Vaßen, O. Guillon, J. Gonzalez-Julian, Molten salt shielded synthesis of oxidation prone materials in air. *Nat. Mater.* **18**, 465–470 (2019).
12. N. I. Baklanova *et al*., Protective ceramic multilayer coatings for carbon fibers. *Surf. Coat. Tech.* **201**, 2313–2319 (2006).
13. T. Piquero, H. Vincent, C. Vincent, J. Bouix, Influence of carbide coatings on the oxidation behavior of carbon fibers. *Carbon* **33**, 455–467 (1995).
14. Q. Liu *et al*., Laser ablation behaviors of SiC–ZrC coated carbon/carbon composites. *Surf. Coat. Tech.* **205**, 4299–4303 (2011).
15. J. N. Clark, D. R. Glasson, S. A. A. Jayaweera, Oxidation of chromium carbide. *Thermochim. Acta* **103**, 193–199 (1986).
16. K. L. Choy, Chemical vapour deposition of coatings. *Prog. Mater. Sci.* **48**, 57–170 (2003).
17. P. Xue, H. Wu, Y. Lu, X. Zhu, Recent progress in molten salt synthesis of low-dimensional perovskite oxide nanostructures, structural characterization, properties, and functional applications: A review. *J. Mater. Sci. Technol.* **34**, 914–930 (2018).
18. S. K. Gupta, Y. Mao, A review on molten salt synthesis of metal oxide nanomaterials: Status, opportunity, and challenge. *Prog. Mater. Sci.* **117**, 100734 (2020).
19. Z. J. Dong *et al*., Fabrication and oxidation resistance of titanium carbide-coated carbon fibres by reacting titanium hydride with carbon fibres in molten salts. *Thin Solid Films* **517**, 3248–3252 (2009).
20. J. Ding, D. Guo, C. Deng, H. Zhu, C. Yu, Low-temperature synthesis of nanocrystalline ZrC coatings on flake graphite by molten salts. *Appl. Surf. Sci.* **407**, 315–321 (2017).
21. S. Masoudifar, M. Bavand-Vandchali, F. Golestani-Fard, A. Nemati, Molten salt synthesis of a SiC coating on graphite flakes for application in refractory castables. *Ceram. Int.* **42**, 11951–11957 (2016).
22. Z. J. Dong *et al*., Fabrication of protective tantalum carbide coatings on carbon fibers using a molten salt method. *Appl. Surf. Sci.* **254**, 5936–5940 (2008).
23. X. Li *et al*., Low-temperature preparation of single crystal titanium carbide nanofibers in molten salts. *Cryst. Growth Des.* **11**, 3122–3129 (2011).
24. Growth behavior of chromium carbide and niobium carbide layers on steel substrate, obtained by salt bath immersion coating process. *Thin Solid Films* **259**, 174–180 (1995).
25. H. O. Pierson, *Handbook of Refractory Carbides and Nitrides* (Noyes Publications, ed. 1, 1996).
26. X. Liu, Z. Wang, S. Zhang, Molten salt synthesis and characterization of titanium carbide-coated graphite flakes for refractory castable Applications. *Int. J. Appl. Ceram. Technol.* **8**, 911–919 (2011).
27. Q. Kang *et al*., Preparation of copper–diamond composites with chromium carbide coatings on diamond particles for heat sink applications. *Appl. Therm. Eng.* **60**, 423–429 (2013).
28. A. O. Kunrath, I. E. Reimanis, J. J. Moore, Combustion synthesis of TiC–Cr3C2 composites. *J. Alloys Compd.* **329**, 131–135 (2001).
29. Z. Zhao *et al*., Synthesis of chromium carbide (Cr3C2) nanopowders by the carbonization of the precursor. *Int. J. Refract. Met. Hard Mater.* **29**, 614–617 (2011).
30. D. E. Wolfe, J. Singh, K. Narasimhan, Synthesis of titanium carbide/chromium carbide multilayers by the co-evaporation of multiple ingots by electron beam physical vapor deposition. *Surf. Coat. Tech.* **160**, 206–218 (2002).
31. P. H. Booker, A. O. Kunrath, M. T. Hepworth, Experimental determination of the ternary diagram of the Ti-Cr-C system. *Acta Mater.* **45**, 1625–1632 (1997).
32. J. D. Roach, Effect of chromium on the oxidation resistance of titanium carbide. *J. Electrochem. Soc.* **98**, 160–165 (1951).
33. T. Arai, S. Moriyama, Growth behavior of chromium carbide and niobium carbide layers on steel substrate, obtained by salt bath immersion coating process. *Thin Solid Films* **259**, 174–180 (1995).
34. G. Ghosh, Thermodynamic and kinetic modeling of the Cr-Ti-V system. *JPE* **23**, 310 (2002).
35. D. D. Himbeault, R. A. Varin, K. Piekarski, Carbon fibers coated with chromium carbide using the liquid metal transfer agent technique. *MTA* **20**, 165–170 (1989).
36. K. Koyama, Y. Hashimoto, S. Omori, Diffusion of carbon in TiC. *Trans. JIM* **16**, 211–218 (1975).
37. H. J. Fan *et al*., Influence of surface diffusion on the formation of hollow nanostructures induced by the Kirkendall effect: The basic concept. *Nano Lett.* **7**, 993–997 (2007).
38. H. J. Fan, U. Gösele, M. Zacharias, formation of nanotubes and hollow nanoparticles based on Kirkendall and diffusion processes: A review. *Small* **3**, 1660–1671 (2007).
39. M. Zhao *et al*., Interfacially reinforced carbon fiber/epoxy composites by grafting melamine onto carbon fibers in supercritical methanol. *RSC Advances* **6**, 29654–29662 (2016).